Equilibrium state of a trapped two-dimensional Bose gas

Steffen P. Rath,[1,*] Tarik Yefsah,[1] Kenneth J. Günter,[1] Marc Cheneau,[1,†] Rémi Desbuquois,[1] Markus Holzmann,[2] Werner Krauth,[3] and Jean Dalibard[1]

[1]*Laboratoire Kastler Brossel, CNRS, Université Pierre et Marie Curie, École Normale Supérieure,
24 rue Lhomond, F-75005 Paris, France*

[2]*Laboratoire de Physique Théorique de la Matière Condensée, CNRS, Université Pierre et Marie Curie,
4 Place Jussieu, F-75005 Paris, France, and Laboratoire de Physique et Modélisation des Milieux Condensés,
CNRS, Université Joseph Fourier, BP 166, F-38042 Grenoble, France*

[3]*Laboratoire de Physique Statistique, CNRS, Université Pierre et Marie Curie, Université Paris Diderot,
École Normale Supérieure, 24 rue Lhomond, F-75005 Paris, France*

We study experimentally and numerically the equilibrium density profiles of a trapped two-dimensional ^{87}Rb Bose gas and investigate the equation of state of the homogeneous system using the local density approximation. We find a clear discrepancy between *in situ* measurements and quantum Monte Carlo simulations, which we attribute to a nonlinear variation of the optical density of the atomic cloud with its spatial density. However, good agreement between experiment and theory is recovered for the density profiles measured after time of flight, taking advantage of their self-similarity in a two-dimensional expansion.

Low-dimensional atomic gases provide stringent tests of the many-body description of quantum matter because thermal or quantum fluctuations play a more important role than for three-dimensional (3D) fluids [1]. These systems are prepared by freezing one or two motional degrees of freedom [2]. For 2D Bose gases, recent experiments [3,4] and corresponding numerical analyses [5,6] gave evidence for a Berezinskii-Kosterlitz-Thouless transition, with a quasi-long-range order of the phase of the gas below a critical temperature.

A remarkable feature of the uniform 2D Bose gas is the scale invariance of its equation of state. For a large domain of parameters, the phase-space density $D = n\lambda^2$ is not an independent function of the chemical potential μ and the temperature T, but depends only on the ratio $\alpha = \mu/k_B T$. Here n is the 2D spatial density and $\lambda = (2\pi\hbar^2/mk_B T)^{1/2}$ is the thermal wavelength. Scale invariance stems from the fact that the interaction strength in 2D is determined by a dimensionless number that is approximately energy independent, $\tilde{g} = \sqrt{8\pi}\, a_{3D}/\ell_z$, where a_{3D} is the scattering length characterizing low-energy interactions in 3D, and ℓ_z is the thickness of the gas along the frozen direction z [for harmonic confinement with frequency ω_z, $\ell_z = (\hbar/m\omega_z)^{1/2}$] [7]. Since interactions provide no energy scale, dimensional analysis implies that D has the form $D = F(\alpha, \tilde{g})$. This holds when $\ell_z \gg a_{3D}$ and applies for all experiments so far.

Here we present results from combined experimental and numerical studies to test this scaling property of the 2D Bose gas. The experiments are performed with ^{87}Rb atoms and the results are compared with quantum Monte Carlo (QMC) simulations. Experimental density distributions are inferred from the absorption of a resonant probe light beam. We investigate both the *in situ* distribution of the gas and the one obtained after a time of flight (TOF) in the *x*-*y* plane. The numerical results confirm the scale invariance and

are in excellent agreement with the prediction based on the equation of state for the uniform 2D gas [8] and on the local density approximation. The measured *in situ* distributions clearly differ from the numerical predictions if we assume a linear relation between the optical density of the cloud and its spatial density n. We point out, however, that the usual single-scattering approximation for the probe beam photons, which is at the basis of this linear relation, is insufficient in our situation. Indeed the interparticle distance in the center of the trap is comparable to k_L^{-1}, where k_L is the wave vector of the probe light. After long TOF durations the densities are considerably lower, and the single-scattering approximation holds. We then recover good agreement between theory and experiment, using a dynamical scaling behavior of the 2D Bose gas confined in a harmonic potential [9].

In our experiment, we first prepare a Bose-condensed gas of $\sim 3 \times 10^5$ ^{87}Rb atoms in the $F = 2$, $m_F = 2$ hyperfine state of the ground level $5\,^2S_{1/2}$. The gas is confined in a magnetic Time-averaged orbiting potential trap [10] at a temperature of 160 nK, obtained through evaporative cooling with a radio-frequency (rf) field. We then add a dipole potential providing strong confinement in the vertical direction. This potential is generated by a laser beam at a wavelength of 532 nm and a power of 1.3 W. The beam passes a holographic plate that imprints a phase of π on its upper half and is focused onto the atoms [11]. There it creates (together with the magnetic trap) the potential illustrated in Fig. 1(a). The vertical and horizontal waists of the beam in the absence of the holographic plate are 5.0 and 140 μm, respectively. The trapping frequencies in the combined potential, measured by exciting the dipole oscillation of the atom cloud, are $\omega_z/2\pi = 3.6\,(3)$ kHz along the vertical axis, leading to $\tilde{g} = 0.146\,(6)$, and $\omega_x/2\pi = 21.0\,(5)$ Hz, and $\omega_y/2\pi = 18.8\,(5)$ Hz in the horizontal plane. For convenience we define $\omega = (\omega_x\omega_y)^{1/2} = 2\pi \times 19.9$ Hz.

The dipole potential is ramped up in 1.5 s and it cuts out a plane of atoms in the center of the original cloud, while the remaining atoms reside in the side wells [Fig. 1(b)]. The
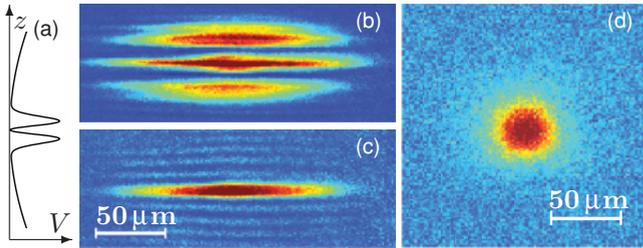
FIG. 1. (Color online) (a) Potential V along the vertical direction z produced by the magnetic trap and the laser beam. (b,c) Side view of the cloud before (b) and after (c) depumping atoms in the side wells. The horizontal stripes are due to diffraction. (d) Top-view *in situ* image yielding fit parameters $T = 132$ nK and $\alpha = 0.29$ (for $\xi = 0.25$).

tunneling between central and side planes is negligible so that the three planes are independent. We depump the side-plane atoms to a nondetected state ($F = 1$) with a 35-ms laser pulse tuned to the $F = 2 \leftrightarrow F' = 2$ transition of the D_2 line, masking the central plane of atoms [Fig. 1(c)]. The atoms are held in the combined trap during 5 s in the presence of the rf, which controls the final temperature.

We probe the spatial density distribution in the *x-y* plane using absorption imaging of a resonant probe laser beam propagating along the vertical axis. The measurement provides a map of the optical density Δ of the atomic cloud, defined as the natural logarithm of the ratio between incident and transmitted light intensities. Neglecting multiple scattering of photons, one has $\Delta(\boldsymbol{r}) = \sigma n(\boldsymbol{r})$, where σ is the absorption cross section. Absorption imaging can be performed in the presence of the trap magnetic field (*in situ* measurement) or after a TOF expansion in the *x-y* plane. A typical *in situ* image is shown in Fig. 1(d). From each image we generate a radial density profile $\Delta(r)$ by averaging over the azimuthal angle while accounting for the residual ellipticity in the *x-y* plane.

We determine μ and T by fitting to the profile $\Delta(r)$ the mean-field Hartree-Fock (MFHF) prediction, which for a strictly 2D gas reads (see, e.g., [12]): $D = -\ln(1 - e^{\alpha - \tilde{g}D/\pi})$. Since our highest temperatures ($\sim$150 nK) are comparable to $\hbar\omega_z/k_B = 170$ nK, the gas is only quasi-2D [13–15] and we take into account corrections to $D(\alpha)$ due to the residual excitation of the atom motion in the z direction [5,13,14,16]. We restrict the fitting domain to simultaneously fulfill two conditions: (i) The phase-space density in the axial ground state must be lower than 2.5 so that beyond-mean-field corrections are negligible [13,17]; (ii) the optical density of the cloud must be lower than 0.2 to exclude distortions due to multiple scattering of probe photons (see later in this article). Because the spatial density enters nonlinearly in the relation between D and α, the fitting procedure can also provide a value of the detection efficiency ξ, defined as the ratio between actual absorption cross section and the ideal one expected for monochromatic probe light in the absence of stray fields. For all images corresponding to a given TOF duration, we extract a single value of ξ from the fit. For *in situ* images, we find the small value $\xi = 0.25\,(4)$, which accounts for the strong reduction of the absorption cross section due to the magnetic field of the trap. With this correction factor, an optical

density of 0.1 corresponds to a density $n \simeq 3.0\,\mu\text{m}^{-2}$. For TOF durations $t \geqslant 10$ ms, all magnetic fields have vanished and we find $\xi = 0.63\,(16)$, consistent with the measured absorption linewidth of the probe laser.

Our path-integral QMC simulations are performed in the canonical ensemble in 3D continuum space for the same geometry as the experiments. They take into account residual excitations along the strongly confined direction z; hence the (small) deformation of the vertical profile [5,18]. Pair interactions are described by a 3D pseudopotential [19]. All thermodynamic properties of the gas are obtained to high precision and without systematic errors. The chemical potential associated to a given atomic distribution is obtained from a fit of the MFHF prediction to the wings of the distribution, as for the experimental data.

We now compare our experimental and numerical results, first confronting the measured *in situ* optical densities with theoretical profiles calculated for the same μ and T. As illustrated in Figs. 2(a) and 2(b), the wings of the calculated and measured profiles nearly coincide, but there is a clear discrepancy in the
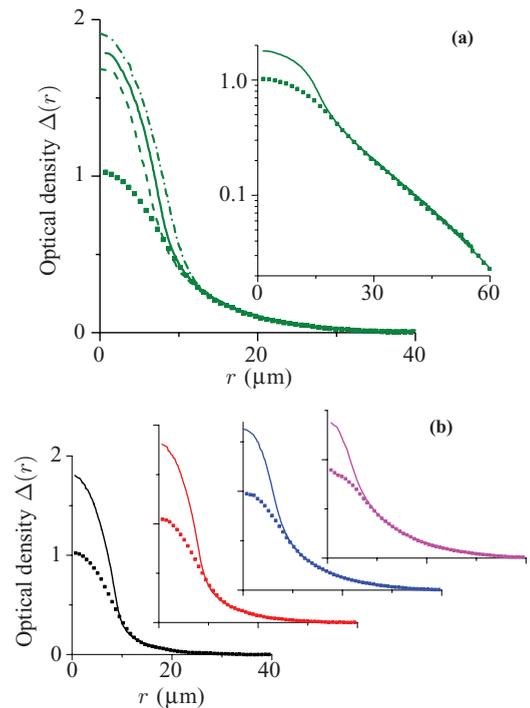
FIG. 2. (Color online) (a) Dots, measured *in situ* optical density profiles $\Delta(r)$. For $\xi = 0.25$ the fit with MFHF theory yields $T = 126\,(6)$ nK, $\alpha = 0.34\,(9)$, where uncertainties represent standard deviations obtained by fitting individual images. Continuous line, corresponding QMC simulation with $N = 73\,900$ atoms (inset, same data in log plot). Upper (dash-dotted) and lower (dashed) lines, QMC results obtained assuming $\xi = 0.21$ [fit parameters $(T\,(\text{nK}),\alpha,N) = (130, 0.39, 96\,300)$] and $\xi = 0.29$ $(122, 0.29, 57\,900)$, respectively. (b) Set of measured density profiles (dots) and corresponding QMC results (lines) for other rf evaporation parameters. From bottom to top: $(T\,(\text{nK}),\alpha,N) = (87, 0.49, 54\,100)$ (black), $(109, 0.39, 63\,800)$ (red), $(142, 0.28, 78\,400)$ (blue), $(153, 0.23, 79\,900)$ (magenta). Each experimental profile in (a) and (b) is an average of nine images.
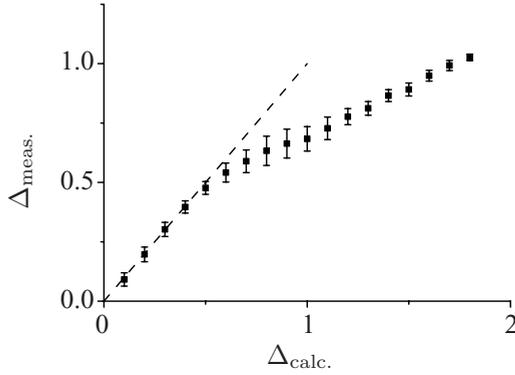
FIG. 3. Measured optical density $\Delta_{\text{meas.}}$ as a function of the calculated optical density $\Delta_{\text{calc.}}$, averaged over the data shown in Figs. 2(a) and 2(b). The dashed line with a slope of 1 is a guide for the eye. Error bars indicate the standard deviation of the data.

central part of the density distributions. Whereas the central optical density in the four coldest experimental distributions is ∼1.0, the QMC simulations systematically predict a central optical density ∼1.8, that is, a density of ∼55 μm^{-2}. A global comparison between predicted and measured Δ is shown in Fig. 3, where we performed an average over the five profiles of Figs. 2(a) and 2(b).

We now discuss possible causes for this discrepancy. A first possible source of error is the uncertainty on the detectivity factor ξ. To estimate its influence, we have reprocessed the measured profile shown in Fig. 2(a) by choosing the lower ($\xi = 0.21$) and upper ($\xi = 0.29$) values of the uncertainty interval for ξ. The QMC results for the modified fit parameters are shown with dash-dotted and dashed lines in Fig. 2(a). Clearly, the uncertainty on ξ does not account for the observed deviation. Other "technical" causes for this discrepancy could be the imperfect resolution of the imaging system and/or the atomic motion during the imaging pulse. However, neither of them can account for the difference between predicted and measured density profiles [20]. The most probable cause of the discrepancy is the reduced absorption cross-section for large 2D atomic densities, due to multiple scattering of the photons of the probe laser beam. Although our optical densities ($\lesssim 1$) do not exceed usual values for absorption imaging, they correspond in this 2D geometry to a short mean distance d between scatterers. For the densest clouds, we find that $k_L d$ is on the order of 1 ($k_L = 8 \times 10^6$ m^{-1}), which can significantly modify the photon scattering rate [21,22].

To relate the trapped gas to a uniform system, we can employ the local density approximation (LDA). Within the LDA, the phase-space density $D(\boldsymbol{r})$ in a trapping potential $V(\boldsymbol{r})$ is given by $D(\boldsymbol{r}) = F(\mu - V(\boldsymbol{r}), T)$, where $D = F(\mu, T)$ is the equation of state of the uniform system. For the quasi-2D Bose gas, the validity of the LDA has been accurately checked with QMC simulations in Ref. [18]. To test the scale invariance of the equation of state, we have plotted in Fig. 4 the phase-space density D as a function of the ratio $\alpha_{\text{local}} \equiv \alpha(r)$ between $\mu - m\omega^2 r^2/2$ and $k_B T$, using the same data as in Figs. 2(a) and 2(b). The calculated functions $D[\alpha(r)]$ (continuous lines) nicely superpose onto each other, confirming the scale invariance in this low-temperature region, where the excitation of the z motion does not play an important role. Note that the central
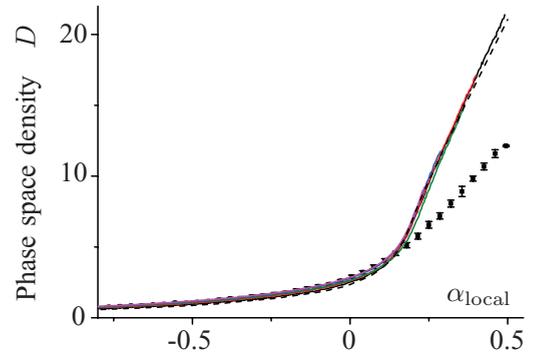
FIG. 4. (Color online) Continuous lines, QMC results for the phase-space density D as a function of $\alpha_{\text{local}} = \alpha - m\omega^2 r^2/k_B T$ for the data shown in Figs. 2(a) and 2(b) (same color code). Black dashed line, prediction of [8] for the uniform case; dots, measured D, averaged over all experimental data shown in Figs. 2(a) and 2(b). Error bars indicate the standard deviation of the data.

phase-space densities notably exceed the critical value for the superfluid transition ($D_c \simeq 8.0$ for $\tilde{g} = 0.146$ [23]), signaling the presence of a significant superfluid component. The QMC results confirm the prediction of [8] for the uniform 2D gas, which was obtained using a classical-field Monte Carlo method (dashed line in Fig. 4). The small corrections to the results of [8] are due to two factors: (i) the presence of residual excitations along the z axis and (ii) the finite value of the interaction parameter $\tilde{g}$ [18]. Obviously, the deviation between experimental and numerical data that was appearing in the density profiles of Figs. 2(a) and 2(b) also shows up in the plot of $D[\alpha(r)]$ in Fig. 4, and the experimental values of D (dots) lie systematically below the predicted ones in the high-phase-space region.

A simple way to circumvent the problem of imaging high-density regions is to take advantage of the dynamical scaling behavior of the 2D Bose gas which manifests itself in a 2D ballistic expansion after a sudden release of the confinement in the x-y plane. It follows from a hidden SO(2,1) symmetry of the 2D Bose gas with contact interactions $U(\boldsymbol{r}) = (\hbar^2 \tilde{g}/m)\delta(\boldsymbol{r})$ when it is confined in an isotropic harmonic potential of frequency ω [9]. Starting from a radially symmetric but otherwise arbitrary initial equilibrium profile $n_{\text{eq}}(r)$, the density profile after a TOF duration t is obtained by a scaling transform

$$n(r,t) = \eta_t^2 \, n_{\text{eq}}(\eta_t r), \quad \eta_t = (1 + \omega^2 t^2)^{-1/2}. \quad (1)$$

This relation was predicted within the Bogoliubov approximation in [24] and holds exactly for interaction potentials that satisfy $U(\lambda \boldsymbol{r}) = U(\boldsymbol{r})/\lambda^2$ [9].

Experimentally, we initiate the 2D expansion by switching off the magnetic trap while keeping the optical potential constant. The atom cloud then expands in the x-y plane for an adjustable duration t, after which we take an image of the cloud. We explore TOF durations up to $t = 14$ ms for which the central density is reduced by a factor $\eta_t^{-2} = 4$, so that artifacts due to multiple scattering of probe photons should be strongly reduced (see Fig. 3). We show in Fig. 5 a succession of density profiles recorded for TOF durations varying from 0 to 14 ms. Each profile has been rescaled to the initial *in situ* distribution
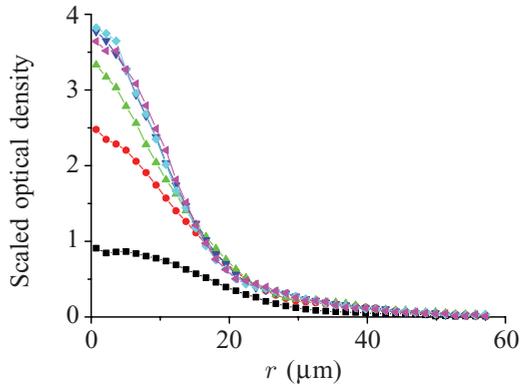
FIG. 5. (Color online) Optical density profiles obtained for TOF durations $t = 0$ ms (black squares), 3 ms (red circles), 6 ms (green up-pointing triangles), 10 ms (blue down-pointing triangles), 12 ms (cyan diamonds), and 14 ms (magenta left-pointing triangles). Each profile has been rescaled to its *in situ* value according to (1).

according to the law (1), so that ideally all profiles should be superimposed. In practice, this superposition is poor for short TOF durations because of (i) the small value of the detection efficiency ξ and (ii) the further reduction of the absorption cross-section due to multiple scattering. The superposition becomes better as the clouds expand and all scaled profiles obtained for $t \geqslant 10$ ms coincide within their noise, as expected from (1). The averaged rescaled data for 10 ms $\leqslant t \leqslant$ 14 ms are plotted in Fig. 6, and are in good agreement with the QMC result.

The observation of this dynamical scaling behavior raises some interesting questions. First, in two dimensions the contact potential needs to be regularized at short distances to avoid ultraviolet divergence. The regularization procedure may lead to deviations with respect to the exact scaling (1) which remain to be investigated. This issue is connected to the problem of the breathing mode of a 2D gas in an isotropic harmonic potential, which should be undamped according to the SO(2,1) dynamical invariance. However, a more recent
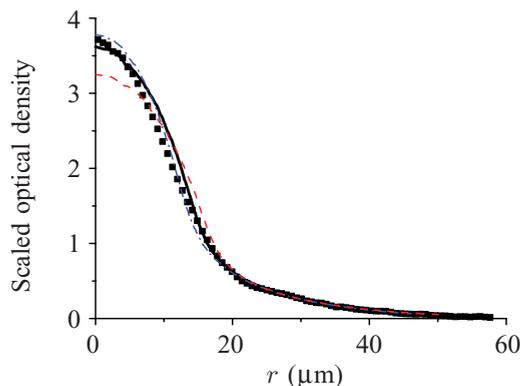
FIG. 6. (Color online) Squares, optical density profile obtained by averaging the experimental data of Fig. 5 for 10 ms $\leqslant t \leqslant$ 14 ms, yielding fit parameters $T = 94$ nK, $\alpha = 0.36$ for $\xi = 0.63$. Lines, QMC results for the same fit parameters (continuous, $N = 42\,000$) and for those deduced assuming $\xi = 0.47$ [dashed red $(T\,(\text{nK}), \alpha, N) = (104, 0.39, 57\,600)$] and $\xi = 0.79$ [dash-dotted blue $(87, 0.33, 32\,100)$].

investigation has found a slight nonexponential damping of the breathing mode due to the production of vortex pairs [25]. Second, the experimentally unavoidable anisotropy of the trapping potential will also cause some deviations from the scaling (1). For highly degenerate clouds, the Bogoliubov approach suggests only small corrections, but it remains to be checked whether this is still true for a cloud with an arbitrary temperature.

The scaling behavior during a 2D expansion is notably different from the properties revealed in a 3D expansion of an initially quasi-2D gas, for which all trapping potentials are switched off simultaneously. In that case, interactions are negligible during the TOF, due to the fast expansion along the initially strongly confined direction. The quasicoherent core which is present below the Berezinskii-Kosterlitz-Thouless transition therefore expands much more slowly than the thermal part of the cloud, leading to multimodal distributions [3,4,26]. By contrast, in the 2D expansion explored in this work, the interaction energy is converted in kinetic energy in the x-y plane and the initial density distribution is entirely preserved except for the mere scaling of (1). The TOF provides a powerful zoom function with magnification η_t, which in principle allows the study of *in situ* spatial correlation functions with an arbitrary resolution.

Two-dimensional and three-dimensional TOF also lead to different expansion rates for the vortices (phase fluctuations) that are present in the critical region at the periphery of the superfluid core. The *in situ* size of a vortex core is the healing length $\xi_{\rm h} = (\tilde{g}n)^{-1/2} \sim 0.4\ \mu$m, corresponding to the momentum scale $\hbar/\xi_{\rm h}$. In a 3D TOF these phase fluctuations are converted into density fluctuations and they can be revealed in absorption imaging after a relatively short TOF duration (the vortex size doubles in a time $\sim m\xi_{\rm h}^2/\hbar \sim 0.2$ ms). By contrast in a 2D TOF, vortices expand at the same rate η_t as the other characteristic lengths of the cloud. In the present case, we would need 2D expansions of $\sim$50 ms in order to reach vortex sizes compatible with the optical resolution of our detection system.

In conclusion, we have studied the equilibrium density profile of a trapped quasi-2D Bose gas. The discrepancy between *in situ* absorption images and numerical calculations suggests that multiple scattering of the probe photons reduces the absorption cross section in high-density regions [22]. To reveal the undistorted density distribution of the gas, we have taken advantage of its self-similarity in a 2D expansion. The profiles measured after this expansion are in good agreement with the QMC predictions. Natural extensions of this work are the measurement of other thermodynamic quantities from *in situ* images using the procedure proposed in [27] and the study of the regime where the scale invariance breaks down and energy-dependent corrections to $\tilde{g}$ become important [17,28–31].

[1] N. D. Mermin and H. Wagner, Phys. Rev. Lett. **17**, 1133 (1966).

[2] A. Görlitz *et al.*, Phys. Rev. Lett. **87**, 130402 (2001).

[3] Z. Hadzibabic *et al.*, Nature (London) **441**, 1118 (2006).

[4] P. Cladé, C. Ryu, A. Ramanathan, K. Helmerson, and W. D. Phillips, Phys. Rev. Lett. **102**, 170401 (2009).

[5] M. Holzmann and W. Krauth, Phys. Rev. Lett. **100**, 190402 (2008).

[6] R. N. Bisset, M. J. Davis, T. P. Simula, and P. B. Blakie, Phys. Rev. A **79**, 033626 (2009).

[7] D. S. Petrov, M. Holzmann, and G. V. Shlyapnikov, Phys. Rev. Lett. **84**, 2551 (2000).

[8] N. V. Prokof'ev and B. V. Svistunov, Phys. Rev. A **66**, 043608 (2002).

[9] L. P. Pitaevskii and A. Rosch, Phys. Rev. A **55**, R853 (1997).

[10] W. Petrich, M. H. Anderson, J. R. Ensher, and E. A. Cornell, Phys. Rev. Lett. **74**, 3352 (1995).

[11] N. L. Smith *et al.*, J. Phys. B **38**, 223 (2005).

[12] Z. Hadzibabic and J. Dalibard, e-print arXiv:0912.1490.

[13] M. Holzmann, M. Chevallier, and W. Krauth, Europhys. Lett. **82**, 30001 (2008).

[14] Z. Hadzibabic *et al.*, New J. Phys. **10**, 045006 (2008).

[15] R. N. Bisset, D. Baillie, and P. B. Blakie, Phys. Rev. A **79**, 013602 (2009).

[16] For our highest densities ($n \sim 60 \, \mu\mathrm{m}^{-2}$), the chemical potential $\mu = \hbar^2 \tilde{g} n/m$ is $\sim$50 nK, notably smaller than $\hbar\omega_z$ (170 nK).

[17] L.-K. Lim, C. M. Smith, and H. T. C. Stoof, Phys. Rev. A **78**, 013634 (2008).

[18] M. Holzmann, M. Chevallier, and W. Krauth, Phys. Rev. A **81**, 043622 (2010).

[19] W. Krauth, Phys. Rev. Lett. **77**, 3695 (1996).

[20] The modeling of our imaging system (triplet lens) yields a point-spread response function with a half width at half maximum value of $\sim$2 μm, much smaller than the typical radius of the gas (20 μm). The transverse displacement of the atoms during the imaging pulse (duration 60 μs) can be accounted for by a convolution of the initial density profile with a Gaussian of width $\lesssim$1.5 μm. Also, their longitudinal displacement $\lesssim$30 μm is too small to significantly defocus the image.

[21] I. M. Sokolov, M. D. Kupriyanova, D. V. Kupriyanov, and M. D. Havey, Phys. Rev. A **79**, 053405 (2009).

[22] A detailed modeling of atom-light interaction in this dense quasi-2D regime will be presented elsewhere.

[23] N. V. Prokof'ev, O. Ruebenacker, and B. V. Svistunov, Phys. Rev. Lett. **87**, 270402 (2001).

[24] Y. Kagan, E. L. Surkov, and G. V. Shlyapnikov, Phys. Rev. A **54**, R1753 (1996).

[25] P. O. Fedichev, U. R. Fischer, and A. Recati, Phys. Rev. A **68**, 011602 (2003).

[26] P. Krüger, Z. Hadzibabic, and J. Dalibard, Phys. Rev. Lett. **99**, 040402 (2007).

[27] T.-L. Ho and Q. Zhou, Nat. Phys. **6**, 131 (2009).

[28] M. Schick, Phys. Rev. A **3**, 1067 (1971).

[29] V. N. Popov, Theor. Math. Phys. **11**, 565 (1972).

[30] C. Mora and Y. Castin, Phys. Rev. Lett. **102**, 180404 (2009).

[31] G. E. Astrakharchik, J. Boronat, J. Casulleras, I. L. Kurbakov, and Y. E. Lozovik, Phys. Rev. A **79**, 051602 (2009).